Journal of Neuroscience Methods 389 (2023) 109794

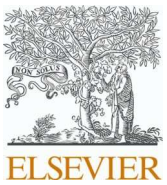

Contents lists available at ScienceDirect

Journal of Neuroscience Methods

journal homepage: www.elsevier.com/locate/jneumeth

A method for estimating and characterizing explicitly nonlinear dynamic functional network connectivity in resting-state fMRI data

S.M. Motlaghian [a,*], V. Vahidi [b], B. Baker [c], A. Belger [d], J.R. Bustillo [e], A. Faghiri [a], J.M. Ford [f,g], A. Iraji [a], K. Lim [h], D.H. Mathalon [f,g], R. Miller [a], B.A. Mueller [h], D. O'Leary [i], S.G. Potkin [j], A. Preda [j], T.G. van Erp [j], V.D. Calhoun [a]

[a] Tri-institutional Center for Translational Research in Neuroimaging and Data Science (Trends), Georgia State, Georgia Tech, and Emory, Atlanta, GA, USA
[b] Department of Computer and Information Science, Spelman College, GA, USA
[c] Tri-institutional Center for Translational Research in Neuroimaging and Data Science (TReNDS), Atlanta, GA Dept. of ECE, Georgia Institute of Technology, Atlanta, GA, USA
[d] Department of Psychiatry, University of North Carolina, Chapel Hill, NC, USA
[e] Department of Psychiatry, University of New Mexico Albuquerque, NM, USA
[f] Department of Psychiatry, University of California San Francisco, San Francisco, CA, USA
[g] San Francisco VA Medical Center, San Francisco, CA, USA
[h] Department of Psychiatry, University of Minnesota, Minneapolis, MN, USA
[i] Department of Psychiatry, University of Iowa, Iowa City, IA, USA
[j] Department of Psychiatry and Human Behavior, University of California Irvine, Irvine, CA, USA

ARTICLE INFO

Keywords:
Mutual information
Explicitly nonlinear
Dynamic nonlinear functional network connectivity
Independent component analysis (ICA)
Intrinsic connectivity networks (ICNs)

ABSTRACT

The past 10 years have seen an explosion of approaches that focus on the study of time-resolved change in functional connectivity (FC). FC characterization among networks at a whole-brain level is frequently termed functional network connectivity (FNC). Time-resolved or dynamic functional network connectivity (dFNC) focuses on the estimation of transient, recurring, whole-brain patterns of FNC. While most approaches in this area have attempted to capture dynamic linear correlation, we are particularly interested in whether explicitly nonlinear relationships, above and beyond linear, are present and contain unique information. This study thus proposes an approach to assess explicitly nonlinear dynamic functional network connectivity (EN dFNC) derived from the relationship among independent component analysis time courses. Linear relationships were removed at each time point to evaluate, typically ignored, explicitly nonlinear dFNC using normalized mutual information (NMI). Simulations showed the proposed method estimated explicitly nonlinearity over time, even within relatively short windows of data. We then, applied our approach on 151 schizophrenia patients, and 163 healthy controls fMRI data and found three unique, highly structured, mostly long-range, functional states that also showed significant group differences. In particular, explicitly nonlinear relationships tend to be more widespread than linear ones. Results also highlighted a state with long range connections to the visual domain, which were significantly reduced in schizophrenia. Overall, this work suggests that quantifying EN dFNC may provide a complementary and potentially valuable tool for studying brain function by exposing relevant variation that is typically ignored.

1. Introduction

Functional connectivity (FC) and its network analog, functional network connectivity (FNC), are widely used to study whole brain resting brain function. These methods study the relationship between time courses (TC) from different brain regions or networks (Allen et al., 2011; Bastos and Schoffelen, 2016; Friston, 2011; Sala-Llonch et al., 2015; van den Heuvel and Hulshoff Pol, 2010).

While most studies attempt to capture linear correlation, though a few studies have evaluated nonlinear brain activity modeling (Lahaye et al., 2003; Stam, 2005; Su et al., 2013; Wismüller et al., 2014). There are few known reasons to expect observing nonlinearity in brain activity

* Corresponding author.
E-mail address: motlaghian86@gmail.com (S.M. Motlaghian).

https://doi.org/10.1016/j.jneumeth.2023.109794
Received 25 December 2022; Accepted 13 January 2023
Available online 15 January 2023

such as nonlinear effects of hemodynamic responses in fMRI data (Deneux and Faugeras, 2006; Miller et al., 2001; Obata et al., 2004), which, crucially, can also vary with time (and location) and changes from subject to subject (de Zwart et al., 2009). Beyond that, the link between neural activity and large-scale brain networks as well as that between networks are extremely complex. Given this there is still considerable work to be done to study the degree of nonlinearity that manifests among brain networks. Our prior work in this direction, identify modular explicitly nonlinear FNC among whole brain networks (Motlaghian et al., 2021). One of the challenges in studying nonlinearity is the linear relationship in FNC often dominants the nonlinear dependencies. As a result, approaches that study the overall relationships (linear + explicitly nonlinear) may not enable us to study the properties of the nonlinear effects (e.g., are they modular, manipulable). To address this in our prior work, we canceled the linear relationship and measured the remaining dependencies (explicitly nonlinear dependencies) using normalized mutual information (NMI) (Motlaghian et al., 2021).

The work mentioned thus far is focused on static measures of functional connectivity, that is measuring temporal coherence averaged across the entire experiment. More recent studies have focused on assessing the dynamics in FNC (dFNC) over time to capture additional insight into the underlying properties of brain activity with the goal to reveal how different areas of the brain interact with each other transiently in a time-resolved analysis. One way to approach this is to divide the time courses into smaller windows and measure the temporal coherence between signals within each successive window. This method is known as the sliding window approach (Allen et al., 2014; Hindriks et al., 2016; Lindquist et al., 2014; Sakoğlu et al., 2010) and is widely used in the field. However, virtually all time-resolved whole brain approaches have focused on changes in the linear dependencies among networks or regions.

The current work is motivated by our prior work (Motlaghian et al., 2021) which identified informative and highly structured explicitly nonlinear relationships in static FNC. Here, our focus is to extend our previous approach to study the dynamic of explicitly nonlinear (EN) dependencies between ICN's time courses and evaluate the properties of these relationships. That is, we are interested in studying the dynamic nonlinear information above and beyond the linear effects, i.e., what is typically ignored in a dynamic linear analysis. We first propose an approach to capture explicitly nonlinear information by removing the linear relationships identified within a sliding window approach, then analyzing the residual, explicitly nonlinear relationships, using normalized mutual information (NMI). To find the appropriate size that suits the sliding window approach, we first show our approach works well within simulated data, including the estimation of NMI over relatively short windows of time. For real fMRI data, we extract the transient nonlinear patterns of FNC and then we evaluate whether these activities show meaningful differences in controls (HC) and patients with schizophrenia (SZ). We present the approach in Section 2.3, then demonstrate it via simulation in Section 2.4. Section 2.5 explained how the proposed method is applied to resting-state fMRI data, including 163 controls and 151 patients. We also compute the linear dFNC and analyze the combination of linear and explicitly nonlinear dFNC findings in Section 2.6. Beyond this, we also validate the results on independent subsets of data to evaluate the replicability of the result. We performed our approach on random subsets of size 100 and 150 (each had 50% HC) individuals to evaluate stability. This assessment shows that state patterns and group effects are consistent and homogenous regardless of the order of subjects and sample subset.

Results showed three distinctive and highly structured EN dynamic states. Several evaluations, such as fractional occupancy, dwell time are performed to study how brain contributes to each state (Section 3.2). The interpretation of these analyses indicates a high level of linear and nonlinear dependency coefficients within and between networks in controls compared to individuals with schizophrenia. We also find significant differences in the concurrence of the linear and explicitly nonlinear states, again highlighting the importance of capturing such, typically ignored, information.

2. Materials and methods

2.1. Quantifying explicitly nonlinear dependency via a normalized mutual information approach

The main aim of this work is to estimate the dynamic of EN dependencies among ICNs, using a sliding window analysis approach (Allen et al., 2014; Hutchison et al., 2013; Hutchison et al., 2013; Saha et al., 2020). For each pair x and y of ICNs, we first estimate the linear correlation measured by a linear model $\bar{y} = \alpha x + \beta$, where $\bar{y}$ is the best linear fit predicting y given x, α is the slope and β is the vertical intercept. Next, the linear effect is removed by calculating $z = y - \bar{y}$. Then dependencies between x and z is measured by normalized mutual information (NMI). There are multiple options to standardize the mutual information, as (Kvalseth, 2017) discussed: 1) min(H(x), H(y)), 2) H(x) + H(y), and 3) max(H(x), H(y)). We employ the latter that is also a (normalized) similarity metric (Horibe, 1985). The formula we use for calculating the value of NMI is

$$\mathrm{NMI}(x,z) = \frac{H(x) + H(z) - H(x,z)}{\max[H(x), H(z)]},$$

where $H(x)$ and, $H(z)$ are marginal entropies and $H(x,z)$ is the joint entropy. The NMI measurement can have values between 0 and 1, if it has a value of 0 this means there is no dependency between x and z, and 1 indicates an absolute dependence of two variables.

We apply the same method for assessing the EN dFNC. Let x_t and $y_t$represent samples of x and y in the window t. Then by linear regression $\bar{y_t} = \alpha_t x_t + \beta_t$, we estimate linear relation between x_t and y_t.Next, the linear effect is removed by calculating $z_t = y_t - \bar{y_t}$. Lastly, dependencies between x_t and z_t is measured by NMI. Swapping x_t and y_t may result in a slightly different value. Thus, we consider the average of both results to ensure symmetry.

2.2. Simulated experiment

The length of the sliding window (number of time points in the window) needed to be wide enough to ensure a reliable estimation of nonlinear dependencies. This size is selected by measuring dependencies in simulated data by NMI. The length was determined using a criterion where NMI can successfully distinguish nonlinear dependency from linear dependency. The impact of the type of the relationship and the number of sample points on NMI are studied in this simulation.

Our focus for the type was on linear and nonlinear dependencies. To do so, we modeled three types of relationships. We created a vector x of size 1000×1 where its components are generated from a random uniform distribution on [0 1], for three cases as follows:

I: Vector y_1 has a purely linear relationship with x.

II: Vector y_2 has a quadratic relationship and no linear correlation with x. That is x and y_2 have only a nonlinear dependency.

III: Vector y_3 has a combination of linear and nonlinear correlation with x.

Gaussian noise of zero mean is added to each equation and plotted in Fig. 1.

We need to ensure the NMI estimation is robust because we are using windowed NMI, which involves a smaller number of time points. To study the impact of the number of data points in the NMI estimation, in each case, we took sample points x_i and y_i of size 35, 50, 75, 100 and measured their relationship before and after removing linear correlation. The dependency before removing linear correlation is represented as MI_1, and dependence after removing linear correlation is measured and represented by MI_2 (Table 1).

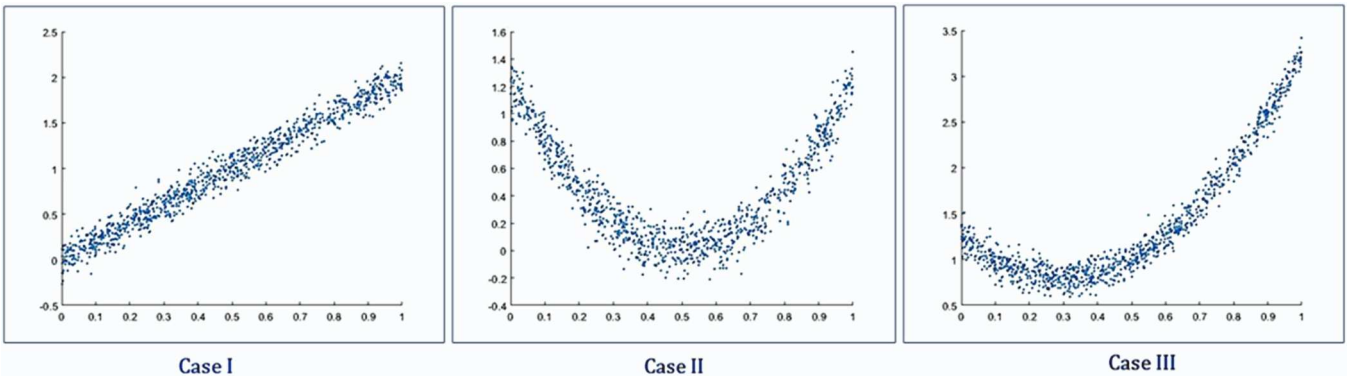

Fig. 1. Three simulations to display linear-only, explicitly nonlinear and linear+nonlinear relationship between two vectors. Vector x is randomly derived from a uniform distribution [0 1]. From left to right, Case I, $y_1 = 2x + \varepsilon$ exhibits an example of a linear-only relationship between x andy_1. In Case II, $y_2 = 5(x - 0.5)^2 + \varepsilon$ which represents an example of an explicitly nonlinear relationship between x andy_2. Case III, $y_3 = 5(x - 0.5)^2 + 2x + \varepsilon$ shows a combination of linear and nonlinear relationships between x and y_3. Noise ε is a Gaussian distribution with a mean of zero.

Table 1
Assessing NMI performance on several samples with 35, 50, 75, and 100 elements in each set for linear-only, explicitly nonlinear, and combination dependencies. Normalized mutual information (NMI) applied on the simulatetion cases represented in Fig. 1. NMI_1 denotes the dependence before linear relationship removal, and NMI_2 represents dependency after linear relationship removal. As the number of sample points gets smaller, the result goes further from ground truth, but the differences between before and after linear removal are still distinguishable. The difference between NMI_1 and NMI_2, and whether these values are near zero is one the identofier of the relationship type.

	T = 35	T = 50	T = 75	T = 100	T = 10,000 (ground truth)
Case I: $\mathbf{y_1 = 2x + \varepsilon}$ (Linear-only relationship)	$NMI_1 = 0.2399$ $NMI_2 = 0.0088$	$NMI_1 = 0.2765$ $NMI_2 = 0.0276$	$NMI_1 = 0.2875$ $NMI_2 = 0.0206$	$NMI_1 = 0.3183$ $NMI_2 = 0.0133$	$NMI_1 = 0.3305$ $NMI_2 = 0.0127$ $NMI_1 >> NMI_2 \sim 0$
Case II: $\mathbf{y_2 = 5(x - 0.5)^2 + \varepsilon}$ (Explicitly Nonlinear relationship)	$NMI_1 = 0.1211$ $NMI_2 = 0.1216$	$NMI_1 = 0.1633$ $NMI_2 = 0.1591$	$NMI_1 = 0.1515$ $NMI_2 = 0.1535$	$NMI_1 = 0.1754$ $NMI_2 = 0.1758$	$NMI_1 = 0.2404$ $NMI_2 = 0.2402$ $NMI_1 \sim NMI_2$
Case III: $\mathbf{y_3 = 5(x - 0.5)^2 + 2x + \varepsilon}$ (Linear and Nonlinear relationships)	$NMI_1 = 0.1558$ $NMI_2 = 0.1176$	$NMI_1 = 0.1748$ $NMI_2 = 0.1385$	$NMI_1 = 0.2431$ $NMI_2 = 0.1606$	$NMI_1 = 0.2419$ $NMI_2 = 0.1777$	$NMI_1 = 0.3001$ $NMI_2 = 0.2357$ $NMI_1 > NMI_2 \neq 0$

2.3. Participants and preprocessing

We used the fBIRN dataset analyzed previously used in (Damaraju et al.). The final curated dataset consisted of 163 healthy participants (mean age 36.9, 117 males; 46 females) and 151 age- and gender-matched patients with schizophrenia (mean age 37.8; 114 males, 37 females). Eyes-closed rsfMRI data were collected at seven sites across the United States (Keator et al., 2016). Informed consent was obtained from all subjects before scanning by the Internal Review Boards of affiliated institutions. Imaging data of one site was captured on a 3-Tesla General Electric Discovery MR750 scanner, and the rest of the six sites were collected on 3-Tesla Siemens Tim Trio scanners. Resting-state fMRI (rsfMRI) scans were acquired using a standard gradient-echo echo-planar imaging paradigm: FOV of 220 × 220 mm (64 × 64 matrices), TR = 2 s, TE = 30 ms, FA = 770, 162 volumes, 32 sequential ascending axial slices of 4 mm thickness and 1 mm skip.

Data preprocessed by using several toolboxes such as AFNI, SPM, GIFT. Rigid body motion correction was applied using the INRIAlign (Freire and Mangin, 2001) toolbox in SPM to correct head motion. To remove the outliers, the AFNI3s 3dDespike algorithm was performed. The rsfMRI data were resampled to 3 mm^3 isotropic voxels. Then data were smoothed to 6 mm full width at half maximum (FWHM) using AFNI3s BlurToFWHM algorithm, and each voxel time course was variance normalized. Subjects with larger movements were excluded from the analysis to mitigate motion effects during the curation process.

2.4. ICA Analysis

The group ICA of fMRI toolbox (GIFT, http://trendscenter.org/software/gift) implementation of Group-level Spatial ICA was used to estimate intrinsic connectivity networks (ICNs). A subject-specific data reduction step was first used to reduce 162 time point data into 100 directions of maximal variability using principal component analysis. After PCA, the infomax approach (Bell and Sejnowski, 1995) was used to estimate 100 maximally independent components from the group PCA reduced matrix. To ensure the stability of the estimation, the ICA algorithm was repeated 20 times, and the most central run was selected as representative (Du et al., 2014). Subject-specific spatial maps (SMs) and time courses (TCs) were obtained using the spatiotemporal regression back reconstruction approach (Calhoun et al., 2001; Erhardt et al., 2011) implemented in the GIFT software.

To label the components, regions of peak activation for each specific spatial map were obtained. After ICA processing, to acquire regions of peak activation, one sample t-test maps are taken for each SM across all subjects and then thresholded; also, mean power spectra of the corresponding TCs were computed. An independent component was identified as an intrinsic connectivity network (ICN) if its peak activation fell within gray matter and has low spatial overlap with known vascular, susceptibility, ventricular, and edge components corresponding to head motion. This results in 47 ICNs out of the 100 independent components.

The ICN time courses were detrended by removing linear, quadratic, and cubic trends and orthogonalized with respect to estimated subject motion parameters. Spikes were detected by AFNI3s 3dDespike algorithm and replaced by values of third-order spline fit. For more detail see (Allen et al., 2012; Damaraju et al., 2014). The fBIRN dataset obtained after processing resulted in a matrix of 159 time points × 47 ICNs × 314 subjects, including 163 Control and 151 SZ subjects. For more details, please see (Damaraju et al.).

2.5. Quantifying (Explicitly Nonlinear) dynamic connectivity in fMRI data

We compared HCs and SZs' states of dynamic functional connectivity (dFNC), using both linear (Pearson correlation) and nonlinear (NMI approach as described in Section 0) dependencies. There are 47 ICN time courses of length 159 time points for each subject. From each time course x, a set of sliding windows x_t, each of length 50 time points, is derived, that is 110 windows in total. To obtain linear dFNC, Pearson correlation between x_t and y_t is evaluated and resulted to 110 symmetric windowed-FNC matrices per individual. To quantify EN dFNC, for each t, the nonlinear dependency of pairs (x_t, y_t) are evaluated as described in Section 2.1, the linear dependency between x_t and y_t removed and then residual dependency is calculated by NMI. This procedure also resulted in 110 symmetric windowed-FNC matrices for each subject (Fig. 2).

We applied the k-means clustering method (using correlation distance) to obtain states for linear and nonlinear dFNC for cluster sizes of k = 2–10. The optimal number of distinct 3 dFNC states was estimated by conducting the elbow method. Final states are achieved by 100 repetitions, as shown in Fig. 3.

After obtaining states, we assessed the group differences. Several quantities are computed at the level of individual's window set and their corresponding K-means indices:

1) Fractional Occupancy (FO)- the percentage of overall time spent in each state.

2) Dwell Time (DT)- average duration of time spent in each state.

Next, we compute a two-sample t-test to compare the differences of these results between controls and schizophrenia patients.

2.6. Relation between linear and nonlinear states

The purpose of this section is to validate the relationship between the three linear and nonlinear states. We first calculated contingency table of simultaneously being in each pair of states for all individuals and then separated the HC's frequencies from SZ. The chi-square test rejects the null hypothesis that the linear and nonlinear dFNC's states are independent (likewise in HC and SZ).

To further evaluate the group differences between the linear and nonlinear state vectors, a contingency table is computed for everyone. Then for each pair of linear and nonlinear states (9 pairs), the differences between HC and SZ are compared by a two-sample t-test.

3. Results

3.1. Simulated experiment

We examined 35, 50, 75, and 100 sample points on simulated data to find an applicable window length that captures nonlinear dependency by implementing the NMI method (Table 1).

In this work, we select 50-time points (100 s) from the result on simulation data (Table 1). This selection is based on two factors. The outcome of using sliding window analysis is sensitive to the length of the sliding window; the length most commonly used in prior studies is between 30 s and 60 s (Allen et al., 2014; Damaraju et al., 2014; Leonardi and Van De Ville, 2015), and in some cases longer (Leonardi and Van De Ville, 2015; Vergara et al., 2019). The other factor to consider is how small this length can be chosen. A small window size may make it difficult to accurately estimate the nonlinearity. The NMI performance on various sample points in Table 1 shows that by taking 50 sample points, NMI can successfully distinguish between the linear-only, explicitly nonlinear and combination relationships as the difference between NMI_1 and NMI_2 are preserved for each case.

3.2. Results from fMRI data

We measured linear and EN dynamic functional connectivity network (dFNC) of 163 healthy controls and 151 schizophrenia patients. The implementation of sliding window analysis and k-means clustering resulted in three states for each linear and nonlinear dFNC. Fig. 3 shows dFNC states and their connectograms for better visualization of the nature of each state.

T-tests were used to identify group differences in several quantities of each linear and nonlinear states between controls and schizophrenic patients. The average fraction occupancy (FO) across healthy controls and schizophrenic patients of each state is calculated and listed in Table 2. The average dwell time (DT) across healthy controls and schizophrenic patients of each state is calculated and reported in Table 3.

Linear states show a high level of positive correlation within networks, and correlation between other networks fluctuates between negative and positive in each linear state. The graphical representations of linear dFNC states show dense interconnectivity within clusters but sparse (or negative in directed graphs) connections between nodes in

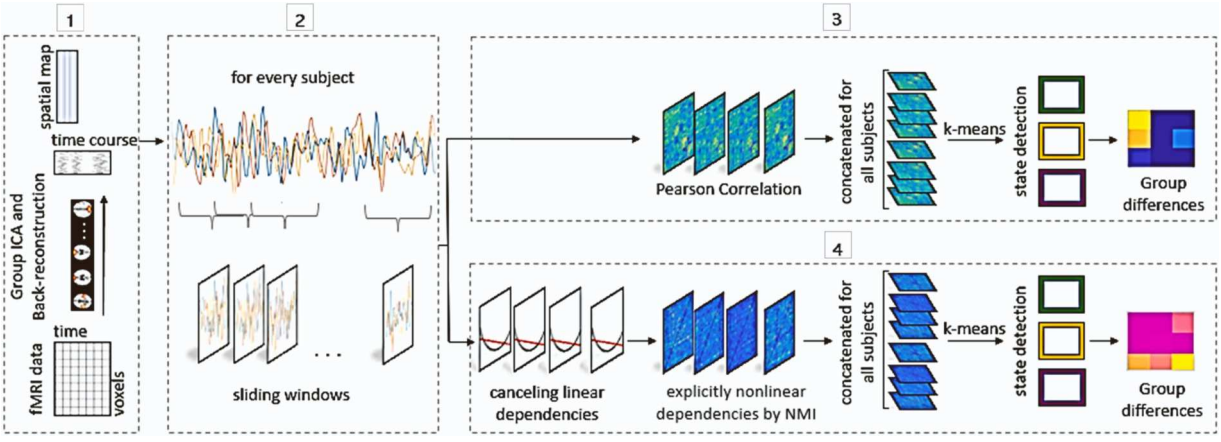

Fig. 2. An overview of the linear and explicitly nonlinear dynamic FNC process. To achieve dFNC states, we took the following steps: 1) Group independent component analysis (ICA) is used to decompose resting-state data from 314 subjects into 100 components, 47 of which are identified as intrinsic connectivity networks (ICNs). Subject-specific spatial maps (SMs) and time courses (TCs) are estimated by the spatiotemporal regression back reconstruction method. 2) Sliding windows of length 50 time points are taken for each subject. 3) (Linear) Dynamic FNC is analyzed. First, the correlation matrices from subject's TCs windows are assessed. Then the matrices are aggregated across all subjects and clustered by k-means clustering. Lastly, to probe the group differences between HC and SZ states are performed. 4) Nonlinear dynamic FNC is analyzed. Steps are identical as (3) except that linear correlation is removed for each window, and the remaining explicitly nonlinear dependencies are assessed by NMI before concatenating step.

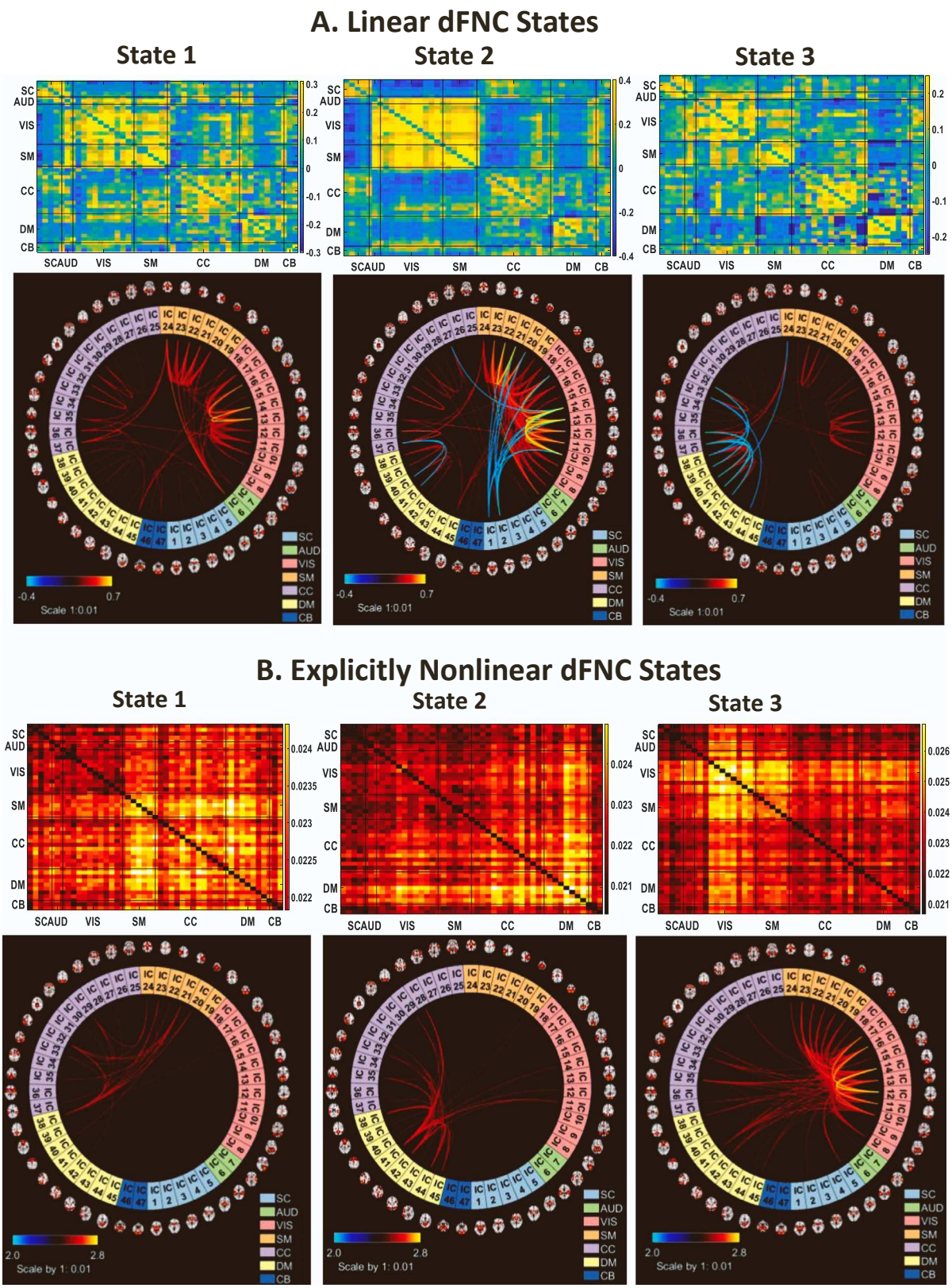

Fig. 3. Linear and explicitly nonlinear states are acquired from the K-means clustering approach for k = 3. Linear and explicitly nonlinear states demonstrate a structured and distinctive contribution in and between networks. The rows of dFNC matrices were partitioned into sub-cortical (SC), auditory (AUD), visual (VIS), sensori-motor (SM), a broad set of regions involved in cognitive control (CC) and attention, default-mode network (DMN) regions, and cerebellar (CB) components. Note that the magnitudes are not the same for states. **A)** States achieved from clustering windows' Pearson correlation of ICNs. The connectograms are thresholded at 0.3. State 2 shows a clear structure with heist magnitude in correlation while state 3 is less structured and shows a lower magnitude of correlation. **B)** States derived from clustering windows' explicitly nonlinear dependencies of ICN's. The connectograms are scaled by 1: 0.01 and thresholded at 0.025. Unlike linear states, the structure of explicitly nonlinear states are unique for each states and exhibits a 'star like' pattern.

Table 2
Fraction Occupancy of HC and SZ in linear and nonlinear dFNC. All linear states and nonlinear state 1 and 3 show highly significant group differences.

Fraction Occupancy of HC and SZ in Linear dFNC State			
	State 1	State 2	State 3
Average across HC	%30	%43	%27
Average across SZ	%14	%21	%65
p-value	6.5383×10^{-5}	2.5613×10^{-7}	1.7319×10^{-14}
Fraction Occupancy of HC and SZ in Nonlinear dFNC			
	State 1	State 2	State 3
Average across HC	%22	%30	%49
Average across SZ	%34	%37	%29
p-value	1.2635×10^{-4}	0.0425	7.3181×10^{-8}

Table 3
Statical analysis of dwell time for linear and nonlinear states in HC and SZ. SZ spends significantly longer in linear state 3.

Dwell Time for HC and SZ in Linear dFNC State			
	State 1	State 2	State 3
Average across HC	54.69	59.08	68.35
Average across SZ	42.16	47.41	151.98
p-value	0.0177	0.0310	5.096×10^{-12}
Dwell Time for HC and SZ in Nonlinear dFNC			
	State 1	State 2	State 3
Average across HC	13.15	12.98	19.52
Average across SZ	17.72	18.23	15.60
p-value	0.0147	0.0051	0.03244

different clusters. State 1 (L1) shows a considerable level of correlation within SC, AUD, VIS, SM, CC, DM networks, and between AUD, VIS, SM networks. However, State 2 (L2) shows a uniformly negative correlation between (AUD, VIS, SM) sets of networks and (CC) but a high level of positive correlation within networks and between AUD, VIS, and SM. State 3 (L3) shows a noticeably smaller range of correlation among all networks.

In the nonlinear dFNC states, we observe a high level of explicitly nonlinear dependencies within a specific network that contributes with broadly all other ICNs. Analogous graphical representations of states 2 and 3 are close to a star graph where only the center node is connected to other nodes. State 1 (NL1) shows high EN dependency in SM and CC (based on the connectogram). State 2 (NL2) shows the EN dependency between DM and other networks, and State 3 (NL3) signifies substantial EN dependencies within VIS and SM and between other networks.

As it is shown in Table 2 and Table 3, HCs spend more time in the VIS and SM system (linear state 2 and nonlinear state 3) compared to patients that spend more frequently and longer in a low range of correlation (linear state 3) in SM, CC and DM networks (nonlinear state 1 and 2) where VIS network's EN dependency has almost vanished.

With this view in Fig. 5, HCs tend to spend longer with a higher probability to EN state 3, which has higher explicitly nonlinear dependencies in VIS and SM. SZ spends longer in higher EN dependency of DM (state 2). The average fraction occupancy for SZ in three explicitly nonlinear states is close to equal, while HC are comparably distributed uniformly. Unlike EN states, the average fraction occupancy of SZ is much higher in linear state 3.

4. Discussion

Dynamic FNC provides a more natural way to analyze uncontrolled resting fMRI data and provide additional insight into brain activity (Hindriks et al., 2016; Hutchison et al., 2013). However, virtually all research in this area, at least at the whole brain/connectome level, has focused on the linear correlation among time courses (Allen et al., 2012; Damaraju et al., 2014; Hutchison et al., 2013; Obata et al., 2004). However, there is considerable evidence of nonlinearity in fMRI data (de Zwart et al., 2009; Sheth et al., 2004; Wan et al., 2006), though very little work has focused on studying the properties of the nonlinear effects after accounting for the largely dominant linear effects. Given that, in this work, we focus on the dynamics of explicitly nonlinear dependency among brain regions.

We measured explicitly nonlinear dFNC and dFNC between TCs obtained from processed fMRI data collected from HC and SZ in this work. Using a k-means classifier, each set of concatenated windows of either Pearson correlation or explicitly nonlinear dependencies are grouped into three integrated patterns of linear dFNC and explicitly nonlinear dFNC (Fig. 3). These states are analyzed, and the differences between HC and SZ in each linear and EN state are compared and studied.

Results suggest that EN states and linear states complement each other as their behavior has basic differences. For example, the average EN dwell time is considerably shorter than the linear dwell time (Fig. 5). These unique aspects can also be observed in the average fraction occupancy.

In the linear states, we observe a strong positive correlation within networks such as (SC), (AUD, VIS, and SM), (CC), (DM), and (CB). For the relation between these networks, it is noted that the correlation swings between negative and positive in each linear state (Fig. 3). Linear state 2 shows a sharp, clear, and intense pattern in terms of correlation between the networks. This pattern fades as moving to linear state 1 and becomes lowest in linear state 3.

For the explicitly nonlinear dFNC states, we measured NMI after removing linear correlation at each window. NMI takes values between 0 and 1. So, we lose the positivity and negativity interpretation here. Multi-network connections were observed in the EN compared to linear dFNC, one predominantly SM (with less but considerable level within CC and DM), one predominantly DM, one predominantly VIS and SM.

Our results (Fig. 4, Fig. 5) indicate that HC tend to have a high level of linear and EN dependencies (linear state 1, 2, and nonlinear state 3). At the same time, SZ tend to stay not only in a lower level of dependencies overall brain networks (linear state 3) but also in the absence of EN dependency in the VIS network (nonlinear state 1 and 2). However, SZ tend to have higher EN dependencies in CC and DM than HC.

These results agree with our earlier findings in evaluating (static) EN FNC (Motlaghian et al., 2021), which indicated significant differences in EN dependencies within and between AUD, VIS, CC, and DM networks in HC and SZ over the entire run. Studying explicitly nonlinear dependencies in dynamic FNC helps unpack the informative structure of how temporally VIS and AUD networks are more active and CC is less involved in HC.

We also analyzed the relationship between fraction occupancy, dwell time of EN states, and symptoms of SZs, and didn't find a significant relationship.

A minor change that would make measuring explicitly nonlinearity more accurate, is the approach for canceling the linear relationship. The best line of fit is not the same when dependent and independent factors switch in linear regression model. Thus, measuring explicitly nonlinear dependencies by canceling linear regression is not symmetric. However, the preference is for being symmetric because we expect to observe the same amount of dependency regardless of the order of inputs. In this work, we found the difference of switching dependent and independent factor to be neglectable, so we addressed non symmetry by taking the average of two results. One can improve the estimation by implementing symmetric linear regression or similar method. Another limitation of using NMI is that the interpretation of positivity and negativity is missed compared to correlation (nonlinear relationships do not always have an interpretable slope as in a linear relationship).

For future work, more investigation of the impact of the window size on the sliding window analysis may drive more information about the dynamic states. The simulation demonstrated NMI showed good

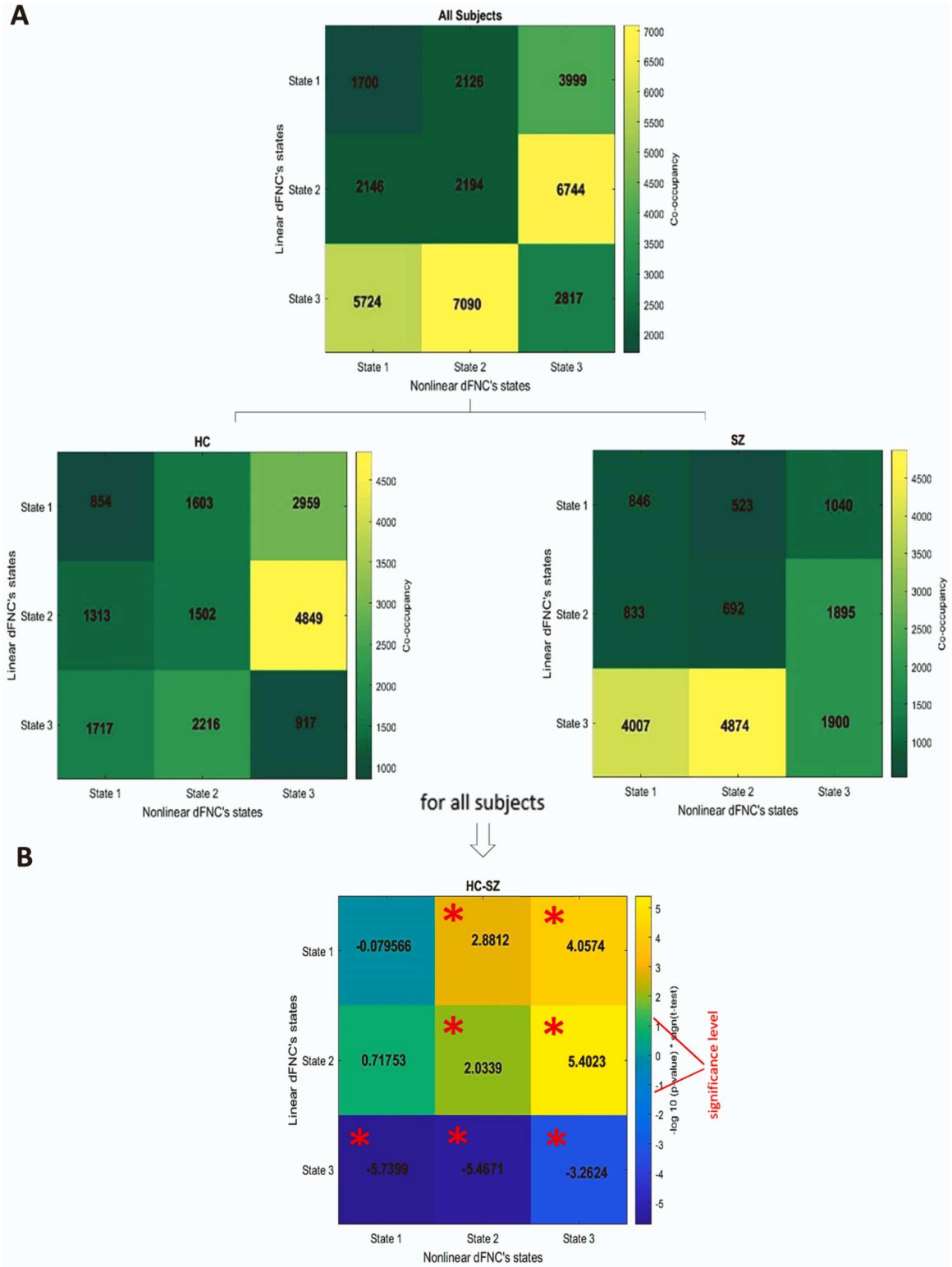

Fig. 4. A) Contingency table of linear and nonlinear dFNC's states for each group shows co-occurrence of states are different between HC and SZ. B) FDR- adjusted p-values from comparing HC-SZ. Significant level indicated by red pointer for alpha= 0.05. HCs are observed significantly more in pairs (2,3) and (1,3), while SZs tend to be in (3,1) and (3,2) of linear-nonlinear states.

performance before and after removing the linear correlation with as few as 35 sample points. In our work, we used 50 time points which can be reduced without losing the NMI sensibility. It would also be interesting to utilize a filter bank approach to cover a larger range of window sizes/frequencies (Faghiri et al., 2021).

Funding sources

This study was funded in part by NIH grants R01MH118695, R01MH123610, and R01EB006841 and NSF grant 2112455.

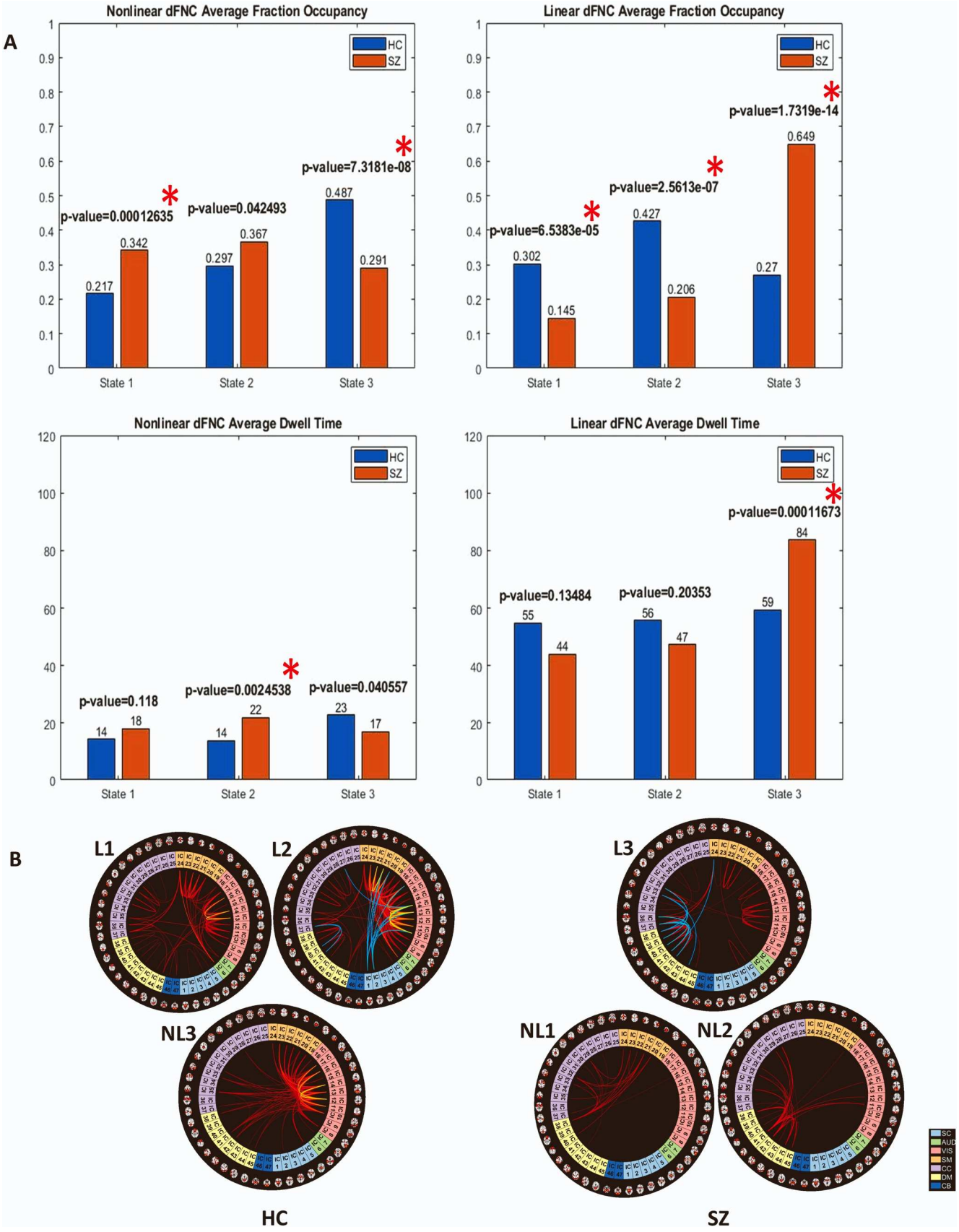

Fig. 5. A) Another representation that shows differences between HC and SZ of fraction occupancy and dwell time. Asterisks denote significant p-values. B) Linear and nonlinear states that HC (left) and SZ (right) spend significantly more time in them. The VIS and SC networks are more active in HC than SZ. Also, in SZ, DM, SM+SC are anticorrelated and the explicitly nonlinear dependency is more activated compared to HC.

CRediT authorship contribution statement

Data collection

A. Belger, J. R. Bustillo, J. M. Ford, K. Lim, D. H. Mathalon, R. Miller, B. A. Mueller, D. O'Leary, S. G. Potkin, A. Preda, T.G. van Erp.

Write manuscript, run analysis

S. M. Motlaghian, V. Vahidi.

Conceptual input

V. D. Calhoun, S. M. Motlaghian, R. Miller, V. Vahidi.

Editing manuscript

B. Baker, A. Belger, J. R. Bustillo, A. Faghiri, J. M. Ford, A. Iraji, K. Lim, D. H. Mathalon, R. Miller, B. A. Mueller, D. O'Leary, G. Pearlson, S. G. Potkin, A. Preda, T.G. van Erp, V. Vahidi, V. D. Calhoun.

Author disclosure statement

No competing financial interests exist.

Data Availability

Data will be made available on request.

References

Allen, E., Erhardt, E., Damaraju, E., Gruner, W., Segall, J., Silva, R., Calhoun, V., 2011. A baseline for the multivariate comparison of resting-state networks. Front. Syst. Neurosci. 5 (2) https://doi.org/10.3389/fnsys.2011.00002.

Allen, E., Damaraju, E., Plis, S., Erhardt, E., Eichele, T., Calhoun, V., 2012. Tracking whole-brain connectivity dynamics in the resting state. Cereb. Cortex *1991*. https://doi.org/10.1093/cercor/bhs352.

Allen, E.A., Damaraju, E., Plis, S.M., Erhardt, E.B., Eichele, T., Calhoun, V.D., 2014. Tracking whole-brain connectivity dynamics in the resting state. Cereb. Cortex 24 (3), 663–676. https://doi.org/10.1093/cercor/bhs352.

Bastos, A.M., Schoffelen, J.-M., 2016. A tutorial review of functional connectivity analysis methods and their interpretational pitfalls. Front. Syst. Neurosci. 9 (175) https://doi.org/10.3389/fnsys.2015.00175.

Bell, A.J., Sejnowski, T.J., 1995. An information-maximization approach to blind separation and blind deconvolution. Neural Comput. 7 (6), 1129–1159. https://doi.org/10.1162/neco.1995.7.6.1129.

Calhoun, V.D., Adali, T., Pearlson, G.D., Pekar, J.J., 2001. A method for making group inferences from functional MRI data using independent component analysis. Hum. Brain Mapp. 14 (3), 140–151. https://doi.org/10.1002/hbm.1048.

Damaraju, E., Allen, E.A., Belger, A., Ford, J.M., McEwen, S., Mathalon, D.H., Calhoun, V.D., 2014. Dynamic functional connectivity analysis reveals transient states of dysconnectivity in schizophrenia. NeuroImage: Clin. 5, 298–308. https://doi.org/10.1016/j.nicl.2014.07.003.

Deneux, T., Faugeras, O., 2006. Using nonlinear models in fMRI data analysis: model selection and activation detection. NeuroImage 32 (4), 1669–1689. https://doi.org/10.1016/j.neuroimage.2006.03.006.

Du, W., Ma, S., Fu, G., Calhoun, V.D., & Adalı, T. (2014, 4–9 May 2014). A novel approach for assessing reliability of ICA for FMRI analysis. Paper presented at the 2014 IEEE International Conference on Acoustics, Speech and Signal Processing (ICASSP).

Erhardt, E.B., Rachakonda, S., Bedrick, E.J., Allen, E.A., Adali, T., Calhoun, V.D., 2011. Comparison of multi-subject ICA methods for analysis of fMRI data. Hum. Brain Mapp. 32 (12), 2075–2095. https://doi.org/10.1002/hbm.21170.

Faghiri, A., Iraji, A., Damaraju, E., Turner, J., Calhoun, V.D., 2021. A unified approach for characterizing static/dynamic connectivity frequency profiles using filter banks. Netw. Neurosci. 5 (1), 56–82. https://doi.org/10.1162/netn_a_00155.

Freire, L., Mangin, J.-F., 2001. Motion correction algorithms may create spurious brain activations in the absence of subject motion. NeuroImage 14, 709–722. https://doi.org/10.1006/nimg.2001.0869.

Friston, K.J., 2011. Functional and effective connectivity: a review. Brain Connect. 1 (1), 13–36. https://doi.org/10.1089/brain.2011.0008.

van den Heuvel, M.P., Hulshoff Pol, H.E., 2010. Exploring the brain network: a review on resting-state fMRI functional connectivity. Eur. Neuropsychopharmacol. 20 (8), 519–534. https://doi.org/10.1016/j.euroneuro.2010.03.008.

Hindriks, R., Adhikari, M.H., Murayama, Y., Ganzetti, M., Mantini, D., Logothetis, N.K., Deco, G., 2016. Can sliding-window correlations reveal dynamic functional connectivity in resting-state fMRI? NeuroImage 127, 242–256. https://doi.org/10.1016/j.neuroimage.2015.11.055.

Horibe, Y., 1985. Entropy and correlation. IEEE Trans. Syst. Man Cybern. 15 (5), 641–642. https://doi.org/10.1109/TSMC.1985.6313441.

Hutchison, R.M., Womelsdorf, T., Allen, E.A., Bandettini, P.A., Calhoun, V.D., Corbetta, M., Chang, C., 2013. Dynamic functional connectivity: promise, issues, and interpretations. NeuroImage 80, 360–378. https://doi.org/10.1016/j.neuroimage.2013.05.079.

Hutchison, R.M., Womelsdorf, T., Gati, J.S., Everling, S., Menon, R.S., 2013. Resting-state networks show dynamic functional connectivity in awake humans and anesthetized macaques. Hum. Brain Mapp. 34 (9), 2154–2177. https://doi.org/10.1002/hbm.22058.

Keator, D.B., van Erp, T.G.M., Turner, J.A., Glover, G.H., Mueller, B.A., Liu, T.T., Potkin, S.G., 2016. The function biomedical informatics research network data repository. NeuroImage 124, 1074–1079. https://doi.org/10.1016/j.neuroimage.2015.09.003.

Kvalseth, T., 2017. On normalized mutual information: measure derivations and properties. Entropy 19, 631. https://doi.org/10.3390/e19110631.

Lahaye, P.J., Poline, J.B., Flandin, G., Dodel, S., Garnero, L., 2003. Functional connectivity: studying nonlinear, delayed interactions between BOLD signals. NeuroImage 20 (2), 962–974. https://doi.org/10.1016/s1053-8119(03)00340-9.

Leonardi, N., Van De Ville, D., 2015. On spurious and real fluctuations of dynamic functional connectivity during rest. NeuroImage 104, 430–436. https://doi.org/10.1016/j.neuroimage.2014.09.007.

Lindquist, M.A., Xu, Y., Nebel, M.B., Caffo, B.S., 2014. Evaluating dynamic bivariate correlations in resting-state fMRI: A comparison study and a new approach. NeuroImage 101, 531–546. https://doi.org/10.1016/j.neuroimage.2014.06.052.

Miller, K.L., Luh, W.-M., Liu, T.T., Martinez, A., Obata, T., Wong, E.C., Buxton, R.B., 2001. Nonlinear temporal dynamics of the cerebral blood flow response. Hum. Brain Mapp. 13 (1), 1–12. https://doi.org/10.1002/hbm.1020.

Motlaghian, S.M., Belger, A., Bustillo, J.R., Ford, J.M., Lim, K., Mathalon, D.H., Calhoun, V.D., 2021. Nonlinear Functional Network Connectivity in Resting Fmri Data, 2021.2007.2020.452982 bioRxiv. https://doi.org/10.1101/2021.07.20.452982.

Obata, T., Liu, T.T., Miller, K.L., Luh, W.-M., Wong, E.C., Frank, L.R., Buxton, R.B., 2004. Discrepancies between BOLD and flow dynamics in primary and supplementary motor areas: application of the balloon model to the interpretation of BOLD transients. NeuroImage 21 (1), 144–153. https://doi.org/10.1016/j.neuroimage.2003.08.040.

Saha, D.K., Damaraju, E., Rashid, B., Abrol, A., Plis, S.M., Calhoun, V.D., 2020. A classification-based approach to estimate the number of resting fMRI dynamic functional connectivity states, 2020.2006.2024.161745 bioRxiv. https://doi.org/10.1101/2020.06.24.161745.

Sakoğlu, U., Pearlson, G.D., Kiehl, K.A., Wang, Y.M., Michael, A.M., Calhoun, V.D., 2010. A method for evaluating dynamic functional network connectivity and task-modulation: application to schizophrenia. Magma 23 (5–6), 351–366. https://doi.org/10.1007/s10334-010-0197-8.

Sala-Llonch, R., Bartrés-Faz, D., Junqué, C., 2015. Reorganization of brain networks in aging: a review of functional connectivity studies. Front. Psychol. 6 (663) https://doi.org/10.3389/fpsyg.2015.00663.

Sheth, S.A., Nemoto, M., Guiou, M., Walker, M., Pouratian, N., Toga, A.W., 2004. Linear and nonlinear relationships between neuronal activity, oxygen metabolism, and hemodynamic responses. Neuron 42 (2), 347–355. https://doi.org/10.1016/S0896-6273(04)00221-1.

Stam, C.J., 2005. Nonlinear dynamical analysis of EEG and MEG: Review of an emerging field. Clin. Neurophysiol. 116 (10), 2266–2301. https://doi.org/10.1016/j.clinph.2005.06.011.

Su, L., Wang, L., Shen, H., Feng, G., Hu, D., 2013. Discriminative analysis of non-linear brain connectivity in schizophrenia: an fMRI Study. Front. Hum. Neurosci. 7, 702. https://doi.org/10.3389/fnhum.2013.00702.

Vergara, V.M., Abrol, A., Calhoun, V.D., 2019. An average sliding window correlation method for dynamic functional connectivity. Hum. Brain Mapp. 40 (7), 2089–2103. https://doi.org/10.1002/hbm.24509.

Wan, X., Riera, J., Iwata, K., Takahashi, M., Wakabayashi, T., Kawashima, R., 2006. The neural basis of the hemodynamic response nonlinearity in human primary visual cortex: implications for neurovascular coupling mechanism. NeuroImage 32 (2), 616–625. https://doi.org/10.1016/j.neuroimage.2006.03.040.

Wismüller, A., Wang, X., Dsouza, A., Nagarajan, M., 2014. A framework for exploring non-linear functional connectivity and causality in the human brain: mutual connectivity. Anal. (MCA) Resting-State Funct. MRI Converg. Cross-Mapp. Non-Metr. Clust.

de Zwart, J.A., van Gelderen, P., Jansma, J.M., Fukunaga, M., Bianciardi, M., Duyn, J.H., 2009. Hemodynamic nonlinearities affect BOLD fMRI response timing and amplitude. NeuroImage 47 (4), 1649–1658. https://doi.org/10.1016/j.neuroimage.2009.06.001.